RSC Advances

ROYAL SOCIETY OF CHEMISTRY

www.rsc.org/advances

$Cu_2(OH)PO_4/g\text{-}C_3N_4$ composite as an efficient visible light-activated photo-Fenton photocatalyst†

Changhong Chen, Yan Zhou, Ningning Wang, Linyu Cheng, Hanming Ding*

School of Chemistry and Molecular Engineering, East China Normal University, 500 Dongchuan Road, Shanghai 200241, China

ABSTRACT: The novel $Cu_2(OH)PO_4/g\text{-}C_3N_4$ composites with different mass percentage of $Cu_2(OH)PO_4$ have been prepared successfully for the photo-Fenton photocatalytic process. By combining the Fenton reagent of $Cu_2(OH)PO_4/H_2O_2$ with the photocatalyst of $g\text{-}C_3N_4$, the Fenton reaction is highly accelerated with the aid of the photocatalytic process. The composite with 30% $Cu_2(OH)PO_4$ shows the best photo-Fenton photocatalytic efficiency with a reaction rate constant of 0.093 min^{-1}, which is about 12 and 2.4 times higher than that of pure $Cu_2(OH)PO_4$ (0.0076 min^{-1}) and pure $g\text{-}C_3N_4$ (0.039 min^{-1}) under the same conditions, respectively. Moreover, the $Cu_2(OH)PO_4/g\text{-}C_3N_4$ composite is very stable and reusable. A possible photo-Fenton photocatalytic reaction mechanism for the $Cu_2(OH)PO_4/g\text{-}C_3N_4$ composite was proposed based on the band structures of $Cu_2(OH)PO_4$ and $g\text{-}C_3N_4$ as well as the previous research results. We confirm that hydroxide radicals and holes play main roles during the photo-Fenton photocatalytic process. Above all, the $Cu_2(OH)PO_4/g\text{-}C_3N_4$ composite as a stable, highly efficient, and economic photo-Fenton photocatalyst shows potential applications for the treatment of organic pollutants in wastewater.

Keywords: $Cu_2(OH)PO_4$; $g\text{-}C_3N_4$; photo-Fenton effect; photocatalysis

* Corresponding author. E-mail: hmding@chem.ecnu.edu.cn; Tel: +86-21-54340061

† Electronic supplementary information (ESI) available: the adsorption curves of RhB over the different catalysts in the dark under stirring, the Fenton and photocatalytic effects of RhB degradation over the different catalysts, the comparison of different effects of RhB degradation over the composite catalyst with 30% $Cu_2(OH)PO_4$, and effects of the initial pH value on RhB degradation.

1. Introduction

Nowadays, advanced oxidation processes (AOPs) such as Fenton reaction, ozonation, photocatalytic oxidation, etc. as the promising treatment methods have been intensively studied by many researchers to remove organic (and sometimes inorganic) materials in wastewater because of their advantages such as safety, simplicity, cleanliness and energy conservation without causing secondary pollution.[1-3] Among the various AOPs, Fenton reaction has been an efficient process proposed for treatment of organic pollutants in toxic effluents.[4, 5] In the traditional homogeneous Fenton process, hydroxyl radicals with violent oxidant capacity are produced by the reaction between Fe(II, III) and H_2O_2.[6, 7] Although the traditional Fenton process can effectively degrade and mineralize organic pollutants in wastewater, Fe(II, III)/H_2O_2 system still has some disadvantages. First, the catalyst is difficult to be recycled and iron ions are hard to be separated from water.[8, 9] Second, the Fenton catalysts can play efficient roles for treatment of wastewater only when the pH value is less than 3.[10, 11] In terms of the reactivity towards H_2O_2, Cu-based Fenton-like catalysts have attracted considerable attention because their redox properties are strikingly similar to Fe-based ones,[12] and can be applied in a broad pH range of 3-9.[13] Copper hydroxide phosphate, $Cu_2(OH)PO_4$ has been proved a promising Fenton reagent because of its unique structure. Libethenite $Cu_2(OH)PO_4$ has an orthorhombic crystal structure with PO_4 tetrahedron, an axially elongated $Cu(1)O_4(OH)_2$ octahedron, an axially compressed $Cu(2)O_4(OH)$ trigonal bipyramid, which usually considered as a catalytic site with high activity, and an OH group between the two Cu species, which could promote H_2O_2 to produce hydroxyl radicals.[14] $Cu_2(OH)PO_4$ has been widely investigated on hydroxylation of phenol by H_2O_2,[15] oxidation of aromatics by H_2O_2,[16] and epoxidation of styrene by H_2O_2 or molecular oxygen.[17] In recent years, it has been reported that $Cu_2(OH)PO_4$ could degrade organic dye in wastewater under ultraviolet (UV),[18] visible[19] and even near-infrared light.[20]

The combination of several AOPs is an efficient way to increase pollutant removal and reduce costs. The coupling of $Cu_2(OH)PO_4$ with semiconductor photocatalysts will

not only increase catalytic efficiency but also recycle the Fenton catalyst. Graphitic carbon nitride (g-C_3N_4) as a π-conjugated material has been proved a particularly interesting photocatalyst because of its merits of easy material availability, simplified preparation, and low cost.[21, 22] Recently, g-C_3N_4 has been reported for photocatalytic water splitting under visible light,[23] organic pollutants degradation and sun energy conversion,[24] etc. And g-C_3N_4 possesses chemical stability and good thermal stability. However, high recombination rate of photogenerated electron-hole pairs limits its further applications in photocatalysis.[25] To solve this problem, several heterojunctions of g-C_3N_4 with other semiconductors of a suitable bandgap have recently been developed to expand the light absorption and improve the separation of photogenerated electron-hole pairs, such as BiOI/g-C_3N_4,[26] Bi_2O_3/g-C_3N_4,[27] Ag_3PO_4/g-C_3N_4,[28, 29] Fe_3O_4/g-C_3N_4,[30] etc. Besides, Cui et al. found that g-C_3N_4 could effectively activate H_2O_2 to generate strong hydroxyl radicals under visible light irradiation, leading to the mineralization of organic dyes.[31] Therefore, it is possible to obtain a photo-Fenton photocatalyst through the combination of $Cu_2(OH)PO_4$ and g-C_3N_4. To our best knowledge, no work has been reported by using the $Cu_2(OH)PO_4$/g-C_3N_4 composite for photo-Fenton photocatalysis under visible light irradiation.

In our current study, we synthesized $Cu_2(OH)PO_4$/g-C_3N_4 composites with different mass percentage of $Cu_2(OH)PO_4$ by the hydrothermal method and focused on their application toward degrading organic pollutants by the photo-Fenton photocatalytic process. The photo-Fenton photocatalytic performance of these composites was evaluated by the degradation of Rhodamine B in the presence of hydrogen peroxide under visible light irradiation. Its kinetics, degradation mechanism, and stability were comprehensively studied.

2. Experimental

2.1. Chemicals

All reagents of urea, $Cu(NO_3)_3 \cdot 3H_2O$, $Na_2HPO_4 \cdot 12H_2O$, NaOH, H_2SO_4, hydrogen peroxide (30 wt.%), and isopropyl alcohol (IPA) were analytical grade and purchased

from Sinopharm Chemical Reagent Co., China. HNO_3 (AR) was obtained from Shanghai Shangsi Fine Chemical Co., Ltd. Rhodamine B (RhB) as a commercial dye was purchased from Xinzhong Chemical Works. *p*-benzoquinone (BQ) and triethanolamine (TEOA) were purchased from Aladin Ltd. (Shanghai, China). All reagents were used without further purification and deionized water was used throughout this study.

2.2. Synthesis of *g*-C_3N_4

Graphitic carbon nitride (*g*-C_3N_4) was prepared by a facile heating urea method.[32] In detail, 10 g of urea was put into an alumina crucible with a cover and then dried in an oven at 80 ºC for 1 h. Then urea was heated to 550 ºC in a Muffle furnace with a PID temperature controller at a heating rate of 10 ºC·min^{-1} and maintained at this temperature for 3 h. The light-yellow *g*-C_3N_4 was obtained after cooling down to the room temperature.

2.3. Synthesis of $Cu_2(OH)PO_4$/*g*-C_3N_4 composites

An appropriate amount of *g*-C_3N_4 was dispersed in 50 mL deionized water and sonicated in an ultrasonic bath for 2 h. Then 5 mmol $Cu(NO_3)_2 \cdot 3H_2O$ was added into the suspension under constant stirring for 1 h and subsequently 2.5 mmol $Na_2HPO_4 \cdot 12H_2O$ was added with constant stirring for 1 h. The pH value of the mixed suspension was adjusted to 7 with 1.0 M NaOH or 1.0 M HNO_3 aqueous solution. The obtained blue suspension was then transferred into a 100 mL Teflon-lined autoclave. The autoclave was sealed and maintained at 120 ºC for 6 h. After cooling to room temperature naturally, the product was collected by centrifugation, then washed with deionized water and ethanol for three times respectively, and finally dried in a drying oven at 60 ºC for 6 h. The samples with different mass fraction of $Cu_2(OH)PO_4$ denoted as 5% $Cu_2(OH)PO_4$, 20% $Cu_2(OH)PO_4$, 30% $Cu_2(OH)PO_4$, and 40% $Cu_2(OH)PO_4$ have been prepared according to the same procedure. Pure $Cu_2(OH)PO_4$ was also obtained by the same method without adding *g*-C_3N_4.[33]

2.5. Characterization

The powder X-ray diffraction (XRD) patterns were obtained on a RiGaku D/Max-RB diffractometer with Cu-Kα radiation (λ=1.5418 Å) in the 2θ range of 10°-80°. UV-vis diffuse reflectance spectra (DRS) were recorded at room temperature by a PerkinElmer Lambda 950 spectrophotometer in the wavelength range of 200-800 nm. Fourier transform infrared spectra (IR) were measured on a Thermo Nicolet Avatar 370 FTIR spectrophotometer with KBr pellet method. Scanning electron microscopy (SEM) and energy dispersive X-ray (EDX) spectroscopy were conducted on a JEOL JEM-100C II electron microscope (Japan).

2.6. Photo-Fenton photocatalytic experiments

The photo-Fenton photocatalytic performance of $Cu_2(OH)PO_4$/*g*-C_3N_4 composites was examined by degrading Rhodamine B (RhB) in the presence of H_2O_2 under visible light irradiation. In detail, 0.02 g of the as-synthesized sample was put into a reactor (double-layer annular glass bottle of 250 mL capacity, the space between the two layers is filled with running water to cool the reaction) with 50 mL of 10 mg/L RhB aqueous solution. The initial pH value of the reaction mixture under native conditions is about 5. All the experiments have been carried out at this pH value if not specifically stated. A 500 W Halogen tungsten lamp with a UV cutoff filter (≥ 410 nm) was used as the visible light source. The reactor was placed ~27 cm away from the light source, and the light intensity was fixed at ~70 mW/cm^2. Prior to illumination, the suspension was continuously stirred in the dark for 30 min at 25 °C to reach an adsorption-desorption equilibrium between the photocatalyst and the dye molecules. Then 1 mL H_2O_2 (30 wt.%) was added into the suspension before switching on the lamp. 3 mL suspension was withdrawn every 10 min interval and centrifuged to remove the photocatalyst. The concentration of the remaining solution was analyzed on a Thermo AquaMate UV-8000 UV-vis spectrophotometer. The stability of the photocatalyst was investigated by repeatedly using the photocatalyst several times. After each photocatalytic reaction, the solid photocatalyst was separated, collected, washed with deionized water, and dried to be reused in the subsequent reaction cycles.

3. Results and discussion

3.1. XRD analysis

Figure 1 shows the powder XRD patterns of pure $Cu_2(OH)PO_4$, pure *g*-C_3N_4 and the $Cu_2(OH)PO_4$/*g*-C_3N_4 composites. It can be found that the XRD pattern of pure $Cu_2(OH)PO_4$ matches well with the orthorhombic phase (JCPDS file no. 36-0404), confirming that the product is Libethenite without any impurities. For pure *g*-C_3N_4, a strong diffraction peak observed at $2\theta = 27.4°$ can be indexed as (002) diffraction plane of graphitic carbon nitride material (JCPDS file no. 87-1526), which is well known for the melon networks.[34] Another weak diffraction peak at $2\theta = 13.1°$ belongs to (100) crystal plane of *g*-C_3N_4 which corresponds to the inter-planar structural packing of the *tri*-s-triazine units.[35] When $Cu_2(OH)PO_4$ was coupled with *g*-C_3N_4, the crystal phase of $Cu_2(OH)PO_4$ and the (002) crystal plane of *g*-C_3N_4 did not change. However, the diffraction peak of *g*-C_3N_4 at $2\theta = 13.1°$ disappeared because the coupling broke the inter-planar structural packing of the *tri*-s-triazine units.[36] Moreover, the diffraction peak intensities of $Cu_2(OH)PO_4$ in $Cu_2(OH)PO_4$/*g*-C_3N_4 composites became stronger when increasing the mass percentage of $Cu_2(OH)PO_4$. In addition, no other impurity peak exits in the XRD patterns, demonstrating that $Cu_2(OH)PO_4$ and *g*-C_3N_4 are the only two phases in the composites.

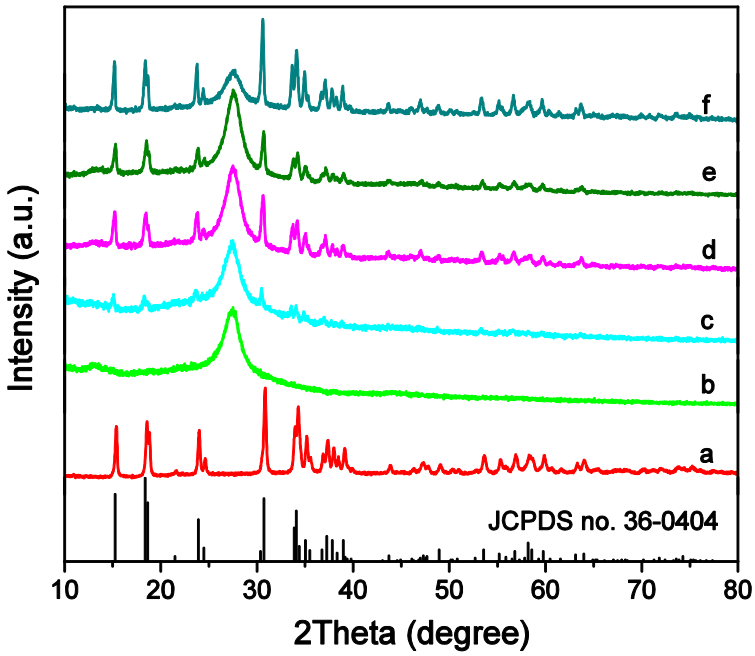

Figure 1. XRD patterns of (a) pure $Cu_2(OH)PO_4$, (b) pure *g*-C_3N_4, (c) 5% $Cu_2(OH)PO_4$, (d) 20% $Cu_2(OH)PO_4$, (e) 30% $Cu_2(OH)PO_4$, and (f) 40% $Cu_2(OH)PO_4$. The bars are from JCPDS file no. 36-0404 for orthorhombic phase of $Cu_2(OH)PO_4$.

3.2. IR analysis

IR spectra of pure $Cu_2(OH)PO_4$, pure *g*-C_3N_4, and the $Cu_2(OH)PO_4$/*g*-C_3N_4 composites are shown in Figure 2. In the case of pure *g*-C_3N_4, the characteristic bands at 1636, 1576, and 1417 cm^{-1} were attributed to typical stretching vibration modes of heptazine-derived repeating units.[37] The vibrational peak at 809 cm^{-1} was assigned to the characteristic ring typical out-of-plane bending vibration of the triazine units.[38] The peaks at 1328 and 1250 cm^{-1} are attributed to the stretching vibrations of C–N(H)–C (partial condensation) or connected units of C–N(–C)–C (full condensation).[39] The broad absorption band at 3182 cm^{-1} for the stretching modes of N–H bonds of primary ($–NH_2$) and secondary (=N–H) amines.[32] In the IR spectrum of $Cu_2(OH)PO_4$, the characteristic bands at 3465 cm^{-1} and 818 cm^{-1} correspond to the stretching and bending modes of the hydroxyls of $Cu_2(OH)PO_4$ and adsorbed water.[40] The vibrational peaks at 962 and 1061 cm^{-1} represent the symmetric and asymmetrical stretching modes of phosphate (ν_1 and ν_3 modes) respectively.[41] The peaks at 656, 634, 609, and 553 cm^{-1} are attributed to ν_4 mode of phosphate. And the peak at 445 cm^{-1} was assigned to the

symmetric distortion vibration of phosphate (ν_2 mode). It can be clearly seen that most of the characteristic peaks of *g*-C_3N_4 and $Cu_2(OH)PO_4$ can be found in $Cu_2(OH)PO_4$/*g*-C_3N_4 composites. However, no significant absorption is observed at 962 and 1061 cm^{-1}, which may arise from the interaction between *g*-C_3N_4 and $Cu_2(OH)PO_4$ through hydrogen bonding between the N-H groups on the surface of *g*-C_3N_4 and phosphate groups of $Cu_2(OH)PO_4$.[42] The formation of H-bonding limits the vibration of stretching modes of phosphate, resulting in the decreased band intensities of ν_1 and ν_3 modes. The IR results clearly confirm the coexistence of $Cu_2(OH)PO_4$ and *g*-C_3N_4 in the composites and the interactions between *g*-C_3N_4 and $Cu_2(OH)PO_4$.

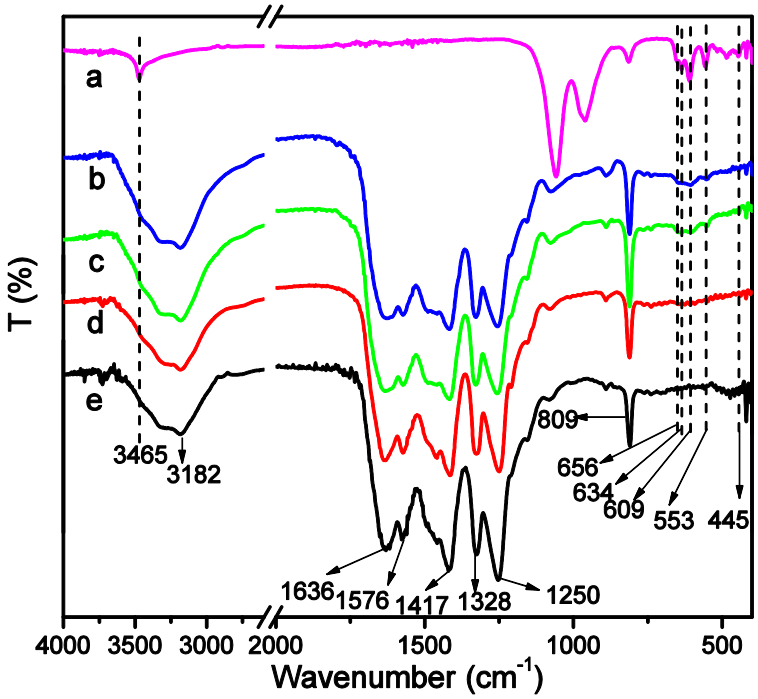

Figure 2. IR spectra of (a) pure $Cu_2(OH)PO_4$, (b) 40% $Cu_2(OH)PO_4$, (c) 30% $Cu_2(OH)PO_4$, (d) 20% $Cu_2(OH)PO_4$, and (e) pure *g*-C_3N_4, respectively.

3.3. SEM analysis

The morphological characteristics of bare *g*-C_3N_4, $Cu_2(OH)PO_4$, and 30% $Cu_2(OH)PO_4$ were shown in Figure 3. A typical lamellar structure and some wrinkles with irregular particles are observed in the bare *g*-C_3N_4 sample (Figure 3A), which are typical morphological characteristic of *g*-C_3N_4 synthesized by the polymerization of

urea.[43] The SEM image of $Cu_2(OH)PO_4$ microcrystals shown in Figure 3B reveals that rod-like superstructure was self-assembled by many irregular nanorods. The morphology of 30% $Cu_2(OH)PO_4$ was shown in Figure 3C. After g-C_3N_4 combined with $Cu_2(OH)PO_4$, the size of *g*-C_3N_4 particles trended to homogenization and the lamellar structure became smaller. Moreover, more irregular nanorods self-assembled to larger rod-like microcrystals. It is obvious to observe that *g*-C_3N_4 has well covered on the surface of $Cu_2(OH)PO_4$. The corresponding energy-dispersive X-ray (EDX) spectrum of 30% $Cu_2(OH)PO_4$ demonstrated the presence of C, N, Cu, O, and P (Figure 3D), which is in agreement with the results of XRD and IR analysis.

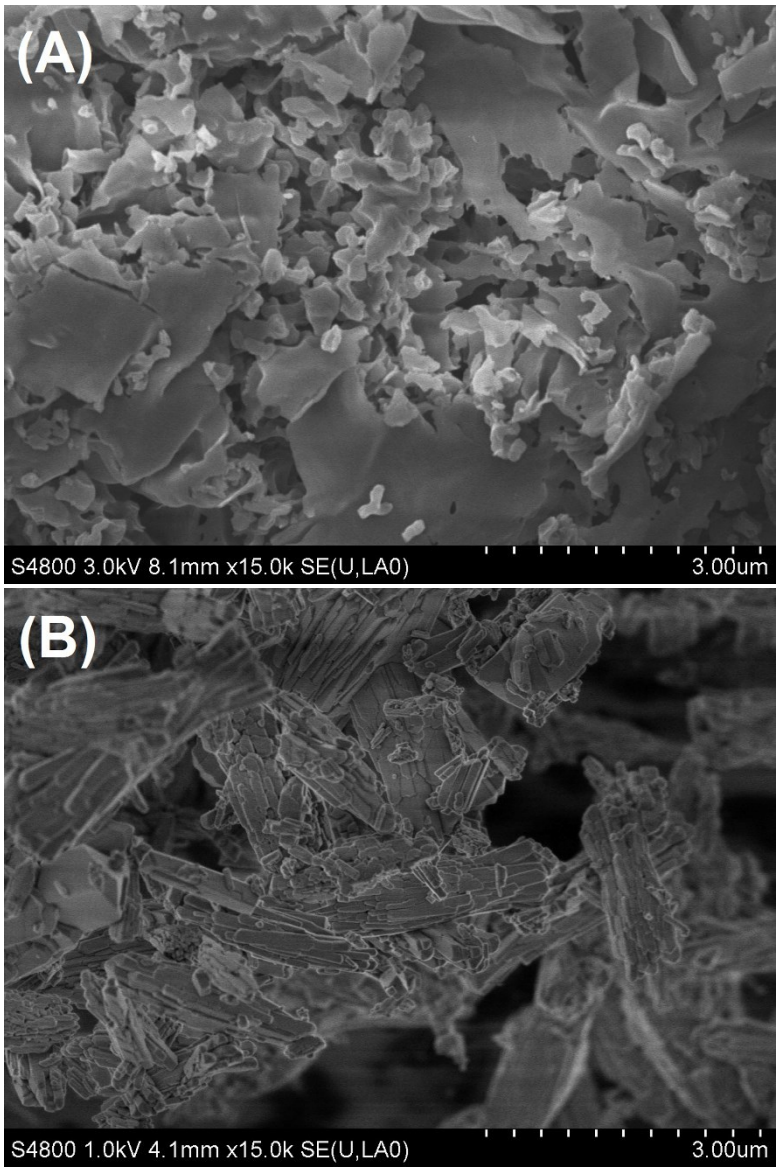

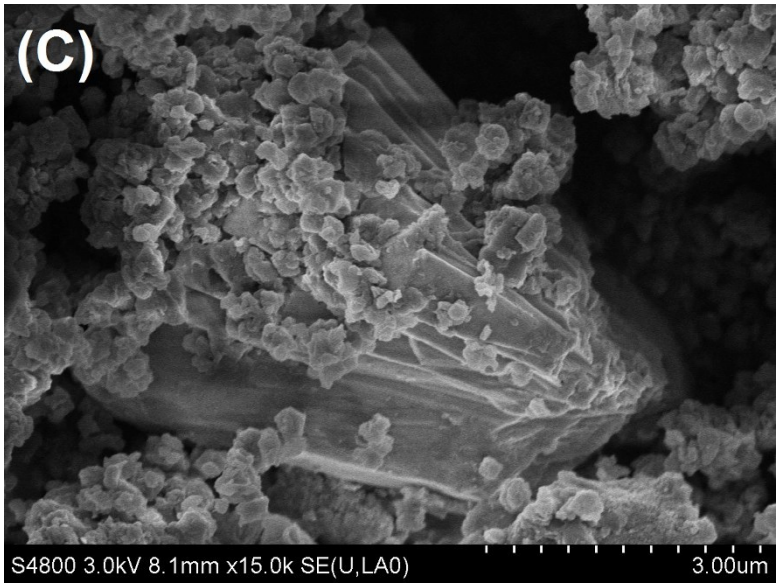

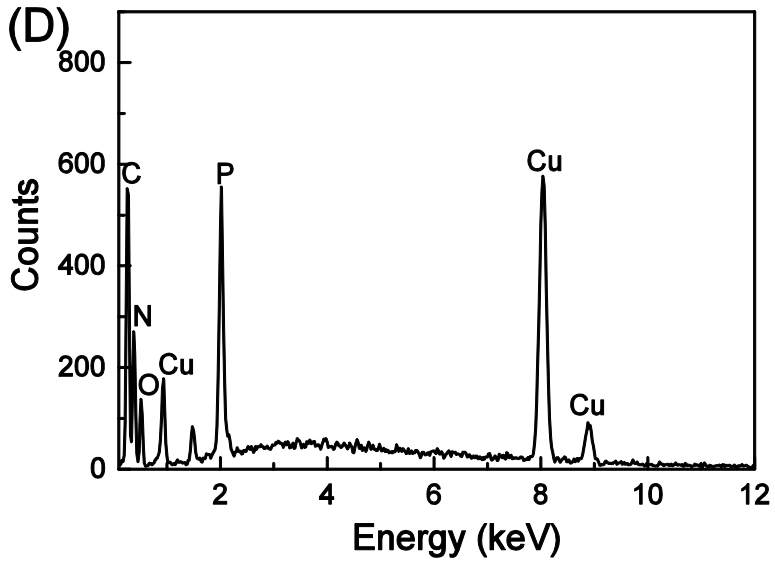

Figure 3. SEM images of (A) pure *g*-C_3N_4, (B) $Cu_2(OH)PO_4$, (C) 30% $Cu_2(OH)PO_4$, and (D) EDX pattern of 30% $Cu_2(OH)PO_4$.

3.4. UV-vis diffuse reflectance spectra

To understand the optical properties of the composites, their corresponding UV-vis reflectance spectra (DRS) are shown in the Figure 4A. It is observed that the absorption edge of $Cu_2(OH)PO_4$ occurs at about 394 nm, which shifts to about 430 nm

in all the $Cu_2(OH)PO_4$/*g*-C_3N_4 composites. Moreover, with the increasing mass percentage of $Cu_2(OH)PO_4$, the absorption at 600-800 nm of the composites is enhanced, which can be due to the high absorption in the NIR region of $Cu_2(OH)PO_4$.[33] The bandgap energies of *g*-C_3N_4, 30% $Cu_2(OH)PO_4$ and pure $Cu_2(OH)PO_4$ are estimated from the intercepts of the tangent lines to the plots according to the following equation: $\alpha h\nu = A(h\nu - E_g)^{n/2}$, where a, ν, E_g and A represent absorption coefficient, light frequency, bandgap energy, and a constant, respectively. The coefficient of n depends on the type of optical transition of a semiconductor (n = 4 for indirect transition). Both *g*-C_3N_4 and $Cu_2(OH)PO_4$ are indirect transition. Therefore, their bandgaps (E_g) can be estimated from the plots of $(\alpha h\nu)^{1/2}$ versus photon energy ($h\nu$), which are shown in Figure 4B. E_g of g-C_3N_4, 30% $Cu_2(OH)PO_4$, and pure $Cu_2(OH)PO_4$ are about 2.65, 2.67, and 2.86 eV, respectively, which are similar to the reported values.[44, 45] The valence band (VB) edge positions and the conduction band (CB) edge positions at the point of zero charge of $Cu_2(OH)PO_4$ and *g*-C_3N_4 can be predicted theoretically from the electronegativity by the following empirical equation: $E_{VB} = X - E_e + 0.5E_g$ and $E_{CB} = E_{VB} - E_g$, where X represents the electronegativity of the semiconductor, E_e is the energy of free electrons on the hydrogen scale (about 4.5 eV).[46] Herein, the E_{VB} and E_{CB} of pure $Cu_2(OH)PO_4$ and *g*-C_3N_4 are shown in Table 1.

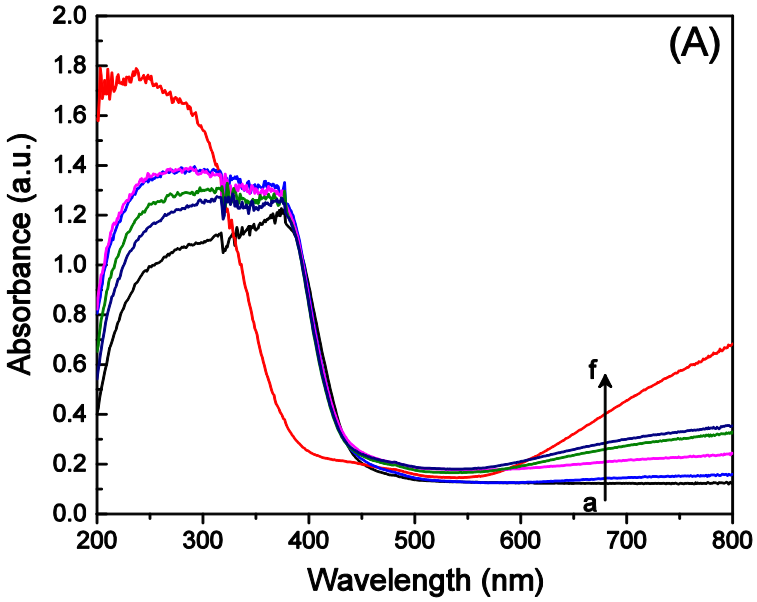

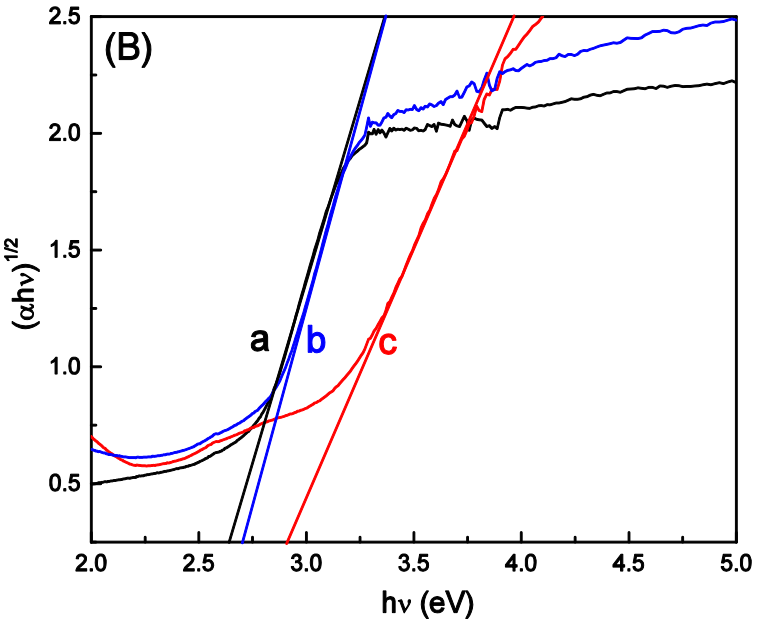

Figure 4. (A) UV-vis diffuse reflectance spectra of (a) pure *g*-C_3N_4, (b) 5% $Cu_2(OH)PO_4$, (c) 20% $Cu_2(OH)PO_4$, (d) 30% $Cu_2(OH)PO_4$, (e) 40% $Cu_2(OH)PO_4$, and (f) pure $Cu_2(OH)PO_4$, respectively. (B) The $(\alpha h\nu)^{1/2}$ versus photon energy ($h\nu$) curves of (a) *g*-C_3N_4, (b) 30% $Cu_2(OH)PO_4$, and (c) pure $Cu_2(OH)PO_4$, respectively.

Table 1. The E_{VB} and E_{CB} of pure $Cu_2(OH)PO_4$ and *g*-C_3N_4.

	X (eV)	Bandgap (eV)	E_{CB} (eV)	E_{VB} (eV)
$Cu_2(OH)PO_4$	4.67	2.86	0.54	3.4
g-C_3N_4	6.47	2.65	-1.15	1.5

3.5. Photo-Fenton photocatalytic performance

Prior to visible light irradiation, the adsorption of RhB molecules over the catalysts was conducted in RhB solution in the dark and the results are given in Figure S1. It can be seen that the adsorption of RhB on all the catalysts proceeds very fast, and reaches an adsorption-desorption equilibrium within 10 min. Except for $Cu_2(OH)PO_4$, the adsorptive capacity of the other catalysts shows a slight difference. By increasing the mass percentage of $Cu_2(OH)PO_4$ in the composite catalysts, the adsorptive capacity has a little decrease, which is associated with the relative poor adsorption ability of $Cu_2(OH)PO_4$. It is noted that the composite catalysts have larger adsorptive capacity

than pure *g*-C_3N_4. This may be because that the *g*-C_3N_4 sheets were further exfoliated to thinner layers when the composite catalysts were prepared under hydrothermal conditions.[47]

The photo-Fenton photocatalytic processes over the different catalysts were carried out in the presence of H_2O_2 under visible light irradiation to evaluate the activity of the $Cu_2(OH)PO_4$/*g*-C_3N_4 composites. As can be seen in Figure 5A, direct photolysis of RhB (blank) and degradation with H_2O_2 under visible light could be neglected. Pure $Cu_2(OH)PO_4$ has a very limited degradation ability with the aid of H_2O_2 under visible light irradiation. However, its degradation ability is highly boosted when coupling with *g*-C_3N_4. The photo-Fenton photocatalytic activity was influenced by the mass percentage of $Cu_2(OH)PO_4$. When the mass percentage of $Cu_2(OH)PO_4$ in the composites was less than 30%, the photo-Fenton photocatalytic effect was enhanced by increasing the mass percentage of $Cu_2(OH)PO_4$. However, when the mass percentage of $Cu_2(OH)PO_4$ was further increased to 40%, the degradation efficiency of RhB was less than that of 30% $Cu_2(OH)PO_4$. Thus 30% $Cu_2(OH)PO_4$ exhibited the best photo-Fenton photocatalytic activity in the present work. This is probably because that the excess $Cu_2(OH)PO_4$ covered on the surface may act as recombination centers for photogenerated electron-hole pairs and prohibit *g*-C_3N_4 from efficient utilization of visible light. As a result, the promotion of *g*-C_3N_4 to the Fenton reaction of $Cu_2(OH)PO_4$ will be restricted. Therefore, the overloaded $Cu_2(OH)PO_4$ in the composite catalysts will have a side effect on the photo-Fenton photocatalytic efficiency.

To better understanding the photo-Fenton photocatalytic reaction kinetics of RhB degradation, the experimental data in Figure 5A were fitted. As shown in Figure 5B, the plots of $\ln(c_0/c)$ versus reaction time are all linear. Thus, all the photo-Fenton photocatalytic reactions follow a pseudo-first-order reaction kinetic. The reaction rate constants (k) are 0.039, 0.0076, 0.058, 0.069, 0.093, and 0.076 min^{-1} for *g*-C_3N_4, $Cu_2(OH)PO_4$, 5% $Cu_2(OH)PO_4$, 20% $Cu_2(OH)PO_4$, 30% $Cu_2(OH)PO_4$, and 40% $Cu_2(OH)PO_4$, respectively. The 30% $Cu_2(OH)PO_4$ shows the best Photo-Fenton photocatalytic effect with the rate constant value 0.093 min^{-1}, which is about 12 and 2.4 times higher than that of pure $Cu_2(OH)PO_4$ and pure *g*-C_3N_4, respectively. The result

further demonstrated that the $Cu_2(OH)PO_4/g\text{-}C_3N_4$ composite is a promising photo-Fenton photocatalyst to degrade organic pollutants.

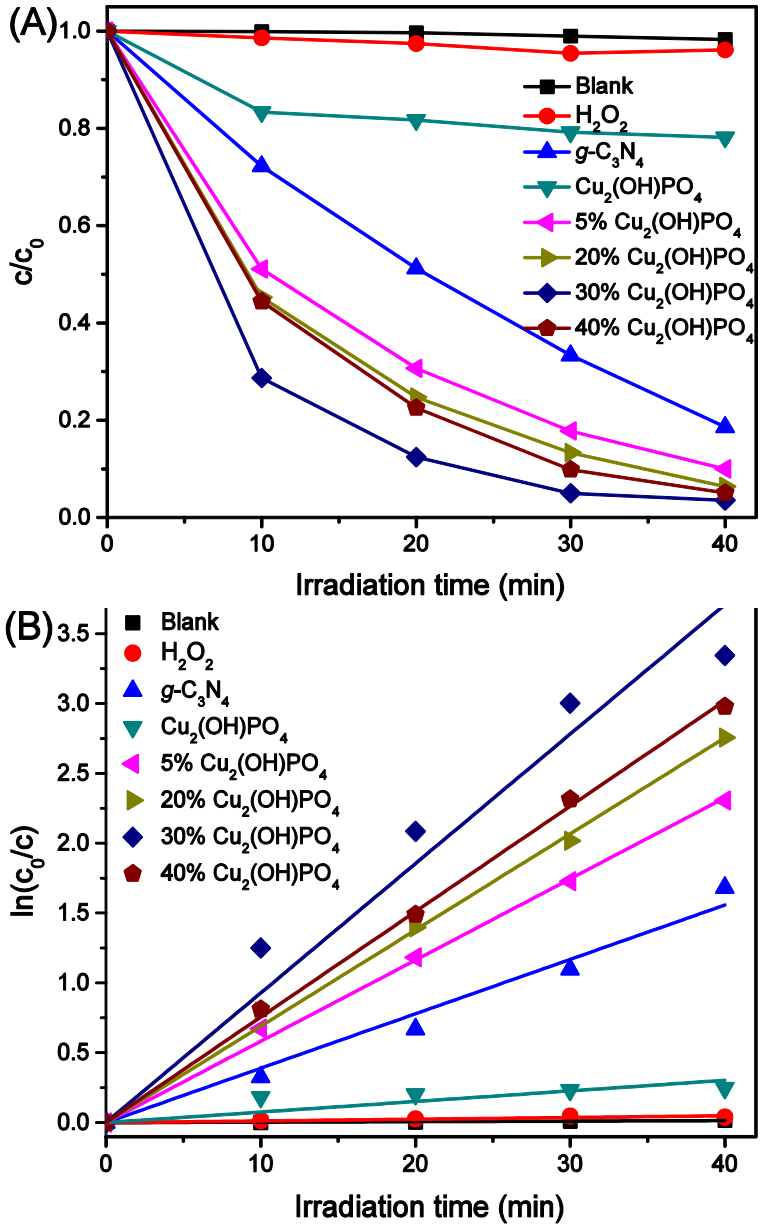

Figure 5. (A) RhB degradation over the different catalysts in the presence of H_2O_2 under visible light irradiation. (B) Kinetics of RhB degradation over the different catalysts in the presence of H_2O_2 under visible light irradiation. The data of direct photolysis (square) and degradation with H_2O_2 (circle) under visible light irradiation are also presented.

The photocatalytic and Fenton degradation reactions over the various catalysts also follow a pseudo-first-order reaction kinetic (Figures S2 and S3). The comparison

of their rate constants is illustrated in Figure 6. As shown in Figure 6, the Fenton reaction rate of pure $Cu_2(OH)PO_4$ is about twice as much as that of *g*-C_3N_4, while the photocatalytic reaction rate of *g*-C_3N_4 is 107 times higher than that of $Cu_2(OH)PO_4$. Therefore, in the $Cu_2(OH)PO_4$/*g*-C_3N_4 composites, the contribution of photocatalytic reactions is mainly attributed to *g*-C_3N_4, while the contribution of Fenton reactions is mainly ascribed to $Cu_2(OH)PO_4$. Pure *g*-C_3N_4 exhibits much higher photocatalytic activity than the $Cu_2(OH)PO_4$/*g*-C_3N_4 composites in the absence of H_2O_2 under visible light irradiation. However, when the Fenton reagent was combined with the photocatalyst in the same reaction system, its Fenton effect is highly enhanced. Even for the composite with 5% $Cu_2(OH)PO_4$, the rate constant of the Fenton reaction increases 7.3 times compared with pure $Cu_2(OH)PO_4$, which should be attributed to a synergistic effect between $Cu_2(OH)PO_4$ and *g*-C_3N_4. Under visible light irradiation, the reaction rate constant is further increased. The overall effect is much greater than the sum of those of Fenton and photocatalytic reactions. The composite with 30% $Cu_2(OH)PO_4$ shows the highest photo-Fenton photocatalytic activity, which is 1.6 times higher than the overall activity of photocatalytic and Fenton reactions. These results demonstrate that the synergetic interaction between $Cu_2(OH)PO_4$ and *g*-C_3N_4 boosts the catalytic efficiency.

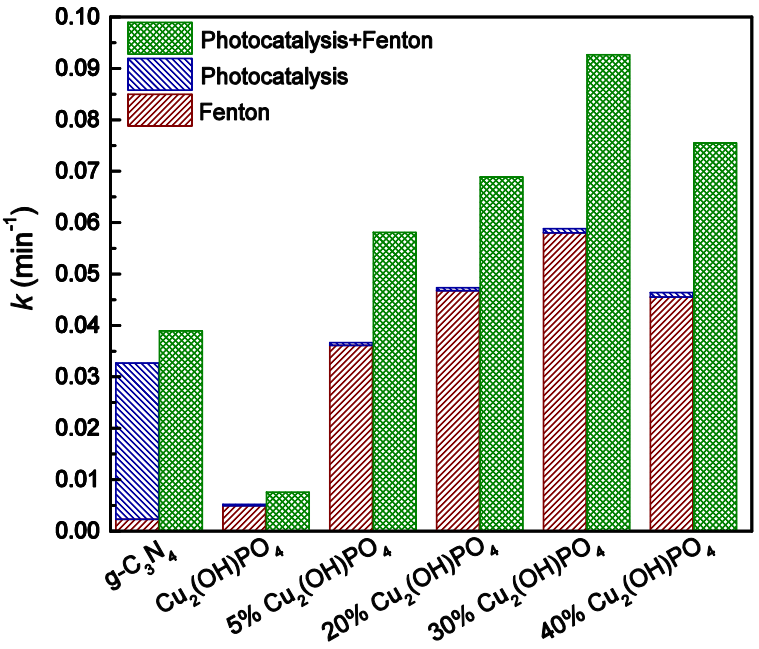

Figure 6. The reaction rate constants of RhB degradation over the $Cu_2(OH)PO_4$/g-C_3N_4 composites with different mass percentage of $Cu_2(OH)PO_4$. Experimental conditions: 0.02 g of catalyst, 50 mL of 10 mg/L RhB aqueous solution, 1 mL H_2O_2 (30 wt.%), 500 W visible light ($\lambda \geq 410$ nm) with an intensity of 70 mW/cm^2, pH 5. "Fenton" in the legend means the reactions happen only in the presence of H_2O_2, "photocatalysis" means only under visible light irradiation, and "photocatalysis + Fenton" means in the presence of H_2O_2 under visible light irradiation.

To further elucidate the photo-Fenton photocatalytic processes, the trapping experiments were carried out to explore the main active species.[48] As shown in Figure 7, it can be easily seen that the catalytic activity of 30% $Cu_2(OH)PO_4$ decreased greatly by adding isopropyl alcohol (IPA) which can trap ·OH radicals. The reaction rate also became smaller by adding triethanolamine (TEOA) which can capture holes. However, there was no obvious change over decomposing efficiency when $\cdot O_2^-$ scavenger, *p*-benzoquinone (BQ) was added. The results of the trapping experiments confirm that ·OH species and photogenerated holes are main oxidative species in the photo-Fenton photocatalytic processes.

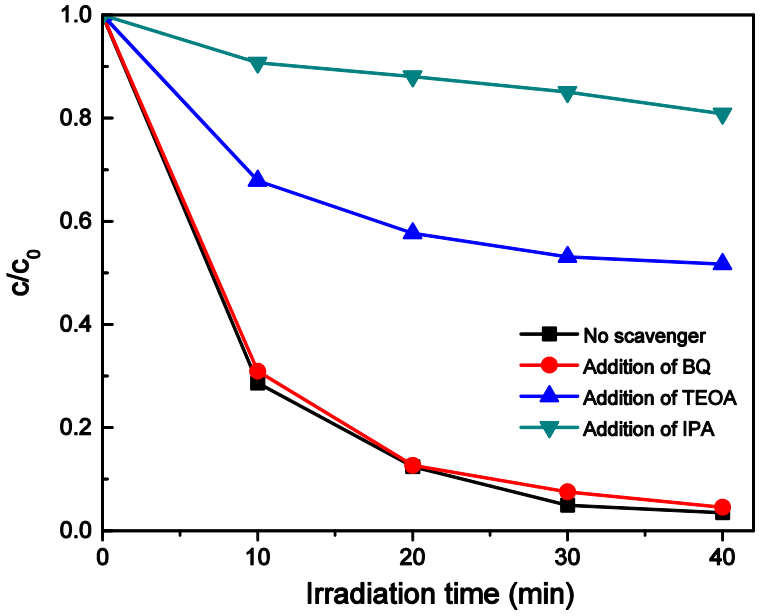

Figure 7. Effect of the different scavengers on RhB degradation over 30% $Cu_2(OH)PO_4$ in presence of H_2O_2 under visible light irradiation.

3.6. Proposed photo-Fenton photocatalytic reaction mechanism for the $Cu_2(OH)PO_4$/*g*-C_3N_4 composites

Based on the above results and the previous reports in the literatures, a possible catalytic mechanism of the $Cu_2(OH)PO_4$/*g*-C_3N_4 composites in the presence of H_2O_2 under visible light irradiation is proposed schematically in Figure 8. It is well known that the photogenerated electrons and holes play important roles in the photocatalytic processes, but depending on their energy levels. The high VB level will weaken the oxidation ability of holes (h^+) and the low CB level will reduce the reduction ability of electrons. As indicated in Figure 8A, both *g*-C_3N_4 and $Cu_2(OH)PO_4$ can be excited under visible light irradiation. The photogenerated electrons will transfer from CB of *g*-C_3N_4 to that of $Cu_2(OH)PO_4$, while the photogenerated holes will transfer from VB of $Cu_2(OH)PO_4$ to that of *g*-C_3N_4 (Eq. 1), as they can form a type-II heterojunction when they are combined together. As a result, the CB electrons in $Cu_2(OH)PO_4$ and the VB holes in *g*-C_3N_4 have decreased reduction and oxidation ability, respectively. As the CB bottom level of $Cu_2(OH)PO_4$ (0.54 eV) is more positive than the redox potential of $O_2/\cdot O_2^-$ (-0.16 eV),[49] the adsorbed O_2 molecules on the surface of the $Cu_2(OH)PO_4$/*g*-C_3N_4 composites cannot be reduced to the superoxide radicals ($\cdot O_2^-$), as illustrated in Figure 8A. This is a possible reason that the $Cu_2(OH)PO_4$/*g*-C_3N_4 composites have much poorer photocatalytic activity than pure *g*-C_3N_4. The high recombination rate of photo-excited electron-hole pairs in $Cu_2(OH)PO_4$ is also responsible for the deterioration.

When H_2O_2 was added, the catalytic activities of the $Cu_2(OH)PO_4$/*g*-C_3N_4 composites were greatly improved even without light irradiation. It is reported that Cu species in $Cu_2(OH)PO_4$ could possibly activate H_2O_2 to produce hydroxyl radicals.[50] The five-coordinated Cu^{II}-OH reacts with H_2O_2 to generate a six-coordinated Cu(II) complex, in which the coordinated H_2O_2 is stabilized by hydrogen-bonding interaction with the coordinated hydroxyl group. Then the Cu(II) complex returns to fivefold coordination by releasing ·OH and H_2O, to produce Cu^{III}-O^-. Cu^{III}-O^- can be converted to Cu^{II}-OH in the presence of reductants or photogenerated electrons in $Cu_2(OH)PO_4$, as demonstrated in Figure 8B. H_2O_2 may be not involved in this reduction process,

otherwise superoxide radicals will be the intermediate species. However, superoxide radicals were not found in the catalytic process as examined in Figure 7. When coupled with *g*-C_3N_4, the Fenton effect of $Cu_2(OH)PO_4$ was greatly enhanced both under visible light irradiation and no light irradiation. Under no light irradiation, the reducible *g*-C_3N_4 surface amino groups may promote the transformation from Cu^{III}-O^- to Cu^{II}-OH in the fourth step shown in Figure 8B (Eq. 7), thus the Fenton reaction can be accelerated in the presence of *g*-C_3N_4. Under visible light illumination, both *g*-C_3N_4 and $Cu_2(OH)PO_4$ can be excited and photogenerated electron-hole pairs are produced. The photogenerated electrons will transfer from VB of *g*-C_3N_4 to that of $Cu_2(OH)PO_4$. These photogenerated electrons can speed up the conversion from Cu^{III}-O^- to Cu^{II}-OH (Eq. 8). Moreover, the photogenerated CB electrons in $Cu_2(OH)PO_4$ are effectively utilized to produce hydroxyl radicals with the aid of a Fenton process (Figure 8B), which cannot be utilized to generate hydroxyl radicals solely in a photocatalytic process. Therefore, the catalytic activity is greatly enhanced when the photocatalytic and Fenton effects are combined in one reaction system. The detailed reaction processes are as follows (Eqs. 1-8).

$$Cu_2(OH)PO_4/g\text{-}C_3N_4 + h\nu \rightarrow g\text{-}C_3N_4\ (h^+) + Cu_2(OH)PO_4\ (e^-) \quad (1)$$

$$h^+ + RhB \rightarrow CO_2 + H_2O \quad (2)$$

$$e^- + H_2O_2 \rightarrow OH^- + \cdot OH \quad (3)$$

$$Cu^{II}\text{-}OH + H_2O_2 \rightarrow Cu^{III}\text{-}O^- + \cdot OH + H_2O \quad (4)$$

$$\cdot OH + RhB \rightarrow CO_2 + H_2O \quad (5)$$

$$Cu^{III}\text{-}O^- + RhB \rightarrow Cu^{II}\text{-}OH + CO_2 + H_2O \quad (6)$$

$$Cu^{III}\text{-}O^- + g\text{-}C_3N_4\text{-}NH_2 \rightarrow Cu^{II}\text{-}OH \text{ (no light irradiation)} \quad (7)$$

$$Cu^{III}\text{-}O^- + H^+ + e^- (h\nu) \rightarrow Cu^{II}\text{-}OH \text{ (under light irradiation)} \quad (8)$$

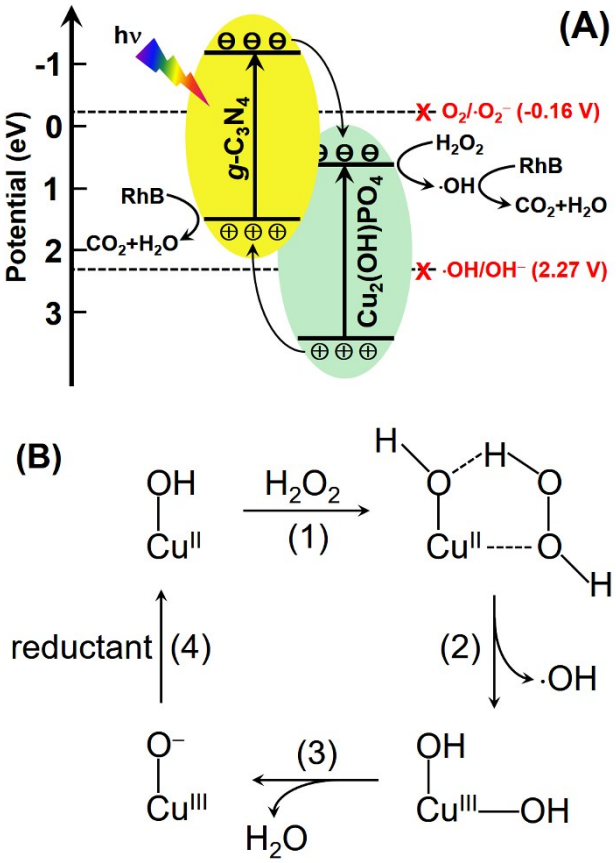

Figure 8. (A) Proposed photo-Fenton photocatalytic reaction mechanism for $Cu_2(OH)PO_4$/g-C_3N_4 composites. (B) The schematic illustration of transformation between Cu(II) and Cu(III) based on the work of Xiao et al.[50]

3.8. Stability of 30% $Cu_2(OH)PO_4$/g-C_3N_4 composite

The stability of catalyst is an important factor of evaluating catalyst that determines whether catalyst can be reused or not. The recycling experiments were carried out to evaluate the reusability of 30% $Cu_2(OH)PO_4$ at the same conditions. As shown in Figure 9A, no apparent reduction of the photo-Fenton activity was observed after five continuous recycles. XRD diffraction patterns of 30% $Cu_2(OH)PO_4$ before and after the photo-Fenton photocatalytic reaction were compared in Figure 9B. No apparent change was observed in the XRD patterns. Moreover, by exploring the effects of the initial pH value on RhB degradation (Figure S5), we can find that our composite catalyst is stable even in the pH range of 3-11, although $Cu_2(OH)PO_4$ is decomposed at pH 11. All the results indicates that the 30% $Cu_2(OH)PO_4$/*g*-C_3N_4 composite is very

stable and re-useable during the photo-Fenton photocatalytic reactions.

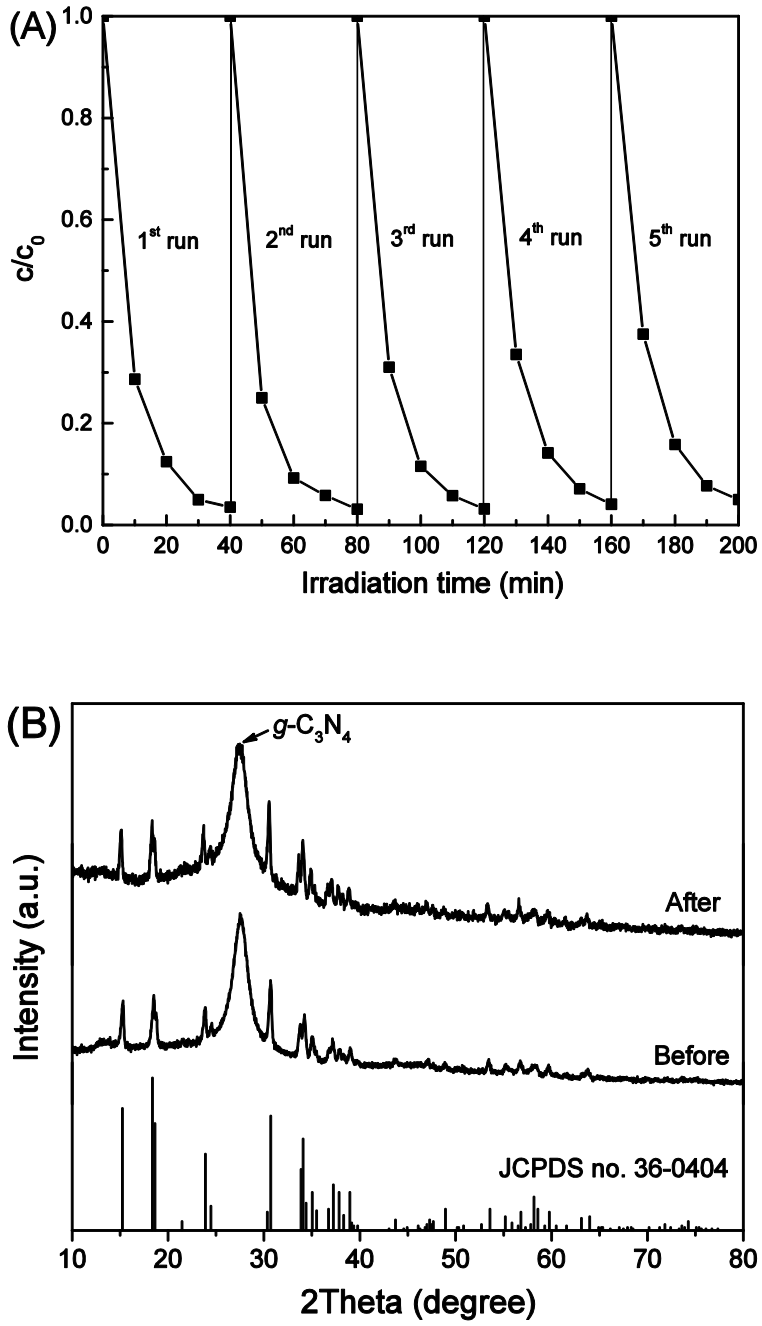

Figure 9. (A) Cycling runs of 30% $Cu_2(OH)PO_4$/*g*-C_3N_4 catalyst for RhB degradation in the presence of H_2O_2 under visible light irradiation. (B) XRD diffraction patterns of (a) fresh 30% $Cu_2(OH)PO_4$ catalyst and (b) used after five runs of photo-Fenton photocatalytic reactions.

4. Conclusions

In summary, we have succeeded preparing the novel $Cu_2(OH)PO_4$/*g*-C_3N_4

composites with different mass percentage of $Cu_2(OH)PO_4$ by the hydrothermal method. By coupling with the photocatalyst of *g*-C_3N_4, the catalytic activity of the Fenton reagent of $Cu_2(OH)PO_4/H_2O_2$ was remarkably improved not only under visible light irradiation but also no light irradiation. The composite with 30% $Cu_2(OH)PO_4$ shows the best photo-Fenton photocatalytic effect with a rate constant of 0.093 min^{-1}, which is about 12 and 2.4 times than those of pure $Cu_2(OH)PO_4$ and pure *g*-C_3N_4 under the same conditions. Moreover, the $Cu_2(OH)PO_4$/*g*-C_3N_4 composite is very stable and reusable during the photo-Fenton photocatalytic reactions. A photo-Fenton photocatalytic reaction mechanism has been proposed for the $Cu_2(OH)PO_4$/*g*-C_3N_4 composite to explain the synergistic effect between $Cu_2(OH)PO_4$ and *g*-C_3N_4. Our finding suggests that the $Cu_2(OH)PO_4$/*g*-C_3N_4 composite can act as a kind of stable, highly efficient, and economic photo-Fenton photocatalyst, which has great superiority for the treatment of non-biodegradable organic pollutants in effluents.

References

1. S. Guo, G. Zhang and J. C. Yu, *J. Colloid Interface Sci.*, 2015, **448**, 460-466.
2. Y. Wang, H. Zhao, M. Li, J. Fan and G. Zhao, *Appl. Catal., B*, 2014, **147**, 534-545.
3. J. Choi, H. Lee, Y. Choi, S. Kim, S. Lee, S. Lee, W. Choi and J. Lee, *Appl. Catal., B*, 2014, **147**, 8-16.
4. J. J. Pignatello, E. Oliveros and A. MacKay, *Crit. Rev. Env. Sci. Tec.*, 2006, **36**, 1-84.
5. A. R. Laiju, T. Sivasankar and P. V. Nidheesh, *Environ. Sci. Pollut. R.*, 2014, **21**, 10900-109007.
6. S. R. Pouran, A. Aziz and W. M. A. W. Daud, *J. Ind. Eng. Chem. (Seoul, Repub. Korea)*, 2015, **21**, 53-69.
7. Y. P. Zhu, T. Z. Ren and Z. Y. Yuan, *Nanoscale*, 2014, **6**, 11395-11402.
8. L. Guo, F. Chen, X. Fan, W. Cai and J. Zhang, *Appl. Catal., B*, 2010, **96**, 162-168.
9. F. Ji, C. Li, J. Zhang and L. Deng, *J. Hazard. Mater.*, 2011, **186**, 1979-1984.
10. X. Li, J. Wang, A. I. Rykov, V. K. Sharma, H. Wei, C. Jin, X. Liu, M. Li, S. Yu, C. Suna and D. D. Dionysioud, *Catal. Sci. Tech.*, 2015, **5**, 504-514.
11. M. I. Pariente, F. Martı´nez, J. A. Melero, J. A. n. Botas, T. Velegraki, N. P. Xekoukoulotakis and D. Mantzavinos, *Appl. Catal., B*, 2008, **85**, 24-32.
12. A. D. Bokare and W. Choi, *J. Hazard. Mater.*, 2014, **275**, 121-135.
13. B. L. Fei, Q. L. Yan, J. H. Wang, Q. B. Liu, J. Y. Long, Y. G. Li, K. Z. Shao and Z. M. S. W. Y. Sun, *Z. Anorg. Allg. Chem.*, 2014, **640**, 2035-2040.
14. A. A. Belik, H. J. Koo, M. H. Whangbo, N. Tsujii, P. e. Naumov and E. Takayama-Muromachimachi, *Inorg. Chem.*, 2007, **46**, 8684-8689.
15. Y. Zhan, H. Li and Y. Chen, *J. Hazard. Mater.*, 2010, **180**, 481-485.
16. X. Meng, Z. Sun, R. Wang, S. Lin, J. Sun, M. Yang, K. Lin, D. Jiang and F. S. Xiao, *Catal.*

Lett., 2001, **76**, 105-108.

17. F. S. Xiao, J. Sun, X. Meng, Ranbo Yu, H. Yuan, D. Jiang, S. Qiu and R. Xu, *Appl. Catal., A*, 2001, **207**, 267-271.

18. L. Ji and R. Yu, *Asia-Pacific Energy Equipment Engineering Research Conference*, Beijing, Apirl, 2015, 224-228.

19. X. Duan, S. Xiao, Y. Liu, H. Huang, D. Wang, L. Wang, B. Liu and T. Wang, *Nat. Nanotechnol.*, 2015, **26**, 031001-031007.

20. S. S. Shah, S. Karthik and N. D. P. Singh, *RSC Adv.*, 2015, **5**, 45416-45419.

21. J. Hong, S. Yin, Y. Pan, J. Han, T. Zhou and R. Xu, *Nanoscale*, 2014, **6**, 14984-14990.

22. J. Liu, Y. Liu, N. Liu, Y. Han, X. Zhang, H. Huang, Y. Lifshitz, S. T. Lee, J. Zhong and Z. Kang, *Science*, 2015, **347**, 970-974.

23. K. Srinivasu, B. Modak and S. K. Ghosh, *J. Phy. Chem. C*, 2014, **118**, 26479-26484.

24. A. Vinu, *Adv. Funct. Mater.*, 2008, **18**, 816-827.

25. J. Theerthagiri, R. A. Senthil, A. Priya, J. Madhavan, R. J. V. Michael and M. Ashokkumarc, *RSC Adv.*, 2014, **4**, 38222-38229.

26. D. Jiang, J. Zhu, M. Chen and J. Xie, *J. Colloid Interface Sci.*, 2014, 147, 115-120.

27. J. Di, J. Xia, S. Yin, H. Xu, L. Xu, Y. Xu, M. He and H. Li, *J. Mater. Chem. A*, 2014, **2**, 5340-5351.

28. D. Jiang, L. Chen, J. Zhu, M. Chen, W. Shi and J. Xie, *Dalton Trans.*, 2013, 42, 15726-15734.

29. Y. He, L. Zhang, B. T. Teng and M. Fan, *Environ. Sci. Technol.*, 2014, **49**, 649-656.

30. S. Kumar, Surendar, B. Kumar, A. Baruah and V. Shanker, *J. Phy. Chem. C*, 2013, **117**, 26135-26143.

31. Y. Cui, Z. Ding, P. Liu, M. Antonietti, X. Fua and X. Wang, *Phys. Chem. Chem. Phys.*, 2012, **14**, 1455-1462.

32. J. Liu, T. Zhang, Z. Wang, G. Dawsona and W. Chen, *J. Mater. Chem.*, 2011, **21**, 14398-14401.

33. G. Wang, B. Huang, X. Ma, Z. Wang, X. Qin, X. Zhang, Y. Dai and M.-H. Whangbo, *Angew. Chem., Int. Ed. Engl.*, 2013, **52**, 4810-4813.

34. X. Wang, K. Maeda, A. Thomas, K. Takanabe, G. Xin, J. M. Carlsson, K. Domen and M. Antonietti, *Nat. Mater.*, 2009, **8**, 76-80.

35. S. Zhang, J. Li, X. Wang, Y. Huang, M. Zeng and J. Xu, *ACS Appl. Mater. Interfaces*, 2014, **6**, 22116-22125.

36. Y. Yao, Y. Cai, F. Lu, J. Qin, F. Wei, C. Xu and S. Wang, *Ind. Eng. Chem. Res.*, 2014, **53**, 17294-17302.

37. Y. Zheng, L. Lin, X. Ye, F. Guo and X. Wang, *Angew. Chem., Int. Ed. Engl.*, 2014, **53**, 11926-119230.

38. Y. Ren, Q. Zhao, X. Li, W. Xiong, M. Tade and L. Liu, *J. Nanopar. Res.*, 2014, **16**, 2532-2539.

39. G. Song, Z. Chu, W. Jin and H. Sun, *Chin. J. Chem. Eng.*, 2015, DOI: 10.1016/j.cjche.2015.05.003.

40. I. S. Cho, D. W. Kim, S. Lee, C. H. Kwak, S. T. Bae, J. H. Noh, S. H. Yoon, H. S. Jung, D. W. Kim and K. S. Hong, *Adv. Funct. Mater.*, 2008, **18**, 2154-2162.

41. R. L. Frost, P. A. Williams, W. Martens, T. Kloprogge and P. Leverett, *J. Raman Spectrosc.*, 2002, **33**, 260-263.

42. S. F. LINCOLN and D. R. STRANK, *Aust. J. Chem.*, 1968, **21**, 37-56.

43. S. Zhou, Y. Liu, J. Li, Y. Wang, G. Jiang, Z. Zhao, D. Wang, A. Duan, J. Liu and Y. Wei, *Appl.*

Catal., B, 2014, **158-159**, 20-29.

44. L. Ye, J. Liu, Z. Jiang, T. Peng and L. Zan, *Appl. Catal., B*, 2013, **142-143**, 1-7.

45. X. Peng, M. Li and C. K. Chan, *J. Phy. Chem. C*, 2015, **119**, 4684-4693.

46. Y. Xu and M. A. A. Schoonen, *Am. Mineral.*, 2015, **85**, 543-556.

47. F. Chang, Y. Xie, J. Zhang, J. Chen, C. Li, J. Wang, J. Luo, B. Deng and X. Hu, *RSC Adv.*, 2014, 4, 28519-28528

48. S. Huang, Y. Xu, M. Xie, H. Xu, M. He, J. Xia, L. Huang and H. Li, *Colloids Surf., A*, 2015, **478**, 71-80.

49. P. M. Wood, *Biochem. J.*, 1988, **253**, 287-289.

50. F.-S. Xiao, J. Sun, X. Meng, R. Yu, H. Yuan, J. Xu, T. Song, D. Jiang and R. Xu, *J. Catal.*, 2001, **199**, 273-281.

Graphical abstract for

$Cu_2(OH)PO_4/g\text{-}C_3N_4$ composite as an efficient visible light-activated photo-Fenton photocatalyst

Changhong Chen, Yan Zhou, Ningning Wang, Linyu Cheng, Hanming Ding*

School of Chemistry and Molecular Engineering, East China Normal University, 500 Dongchuan Road, Shanghai 200241, China

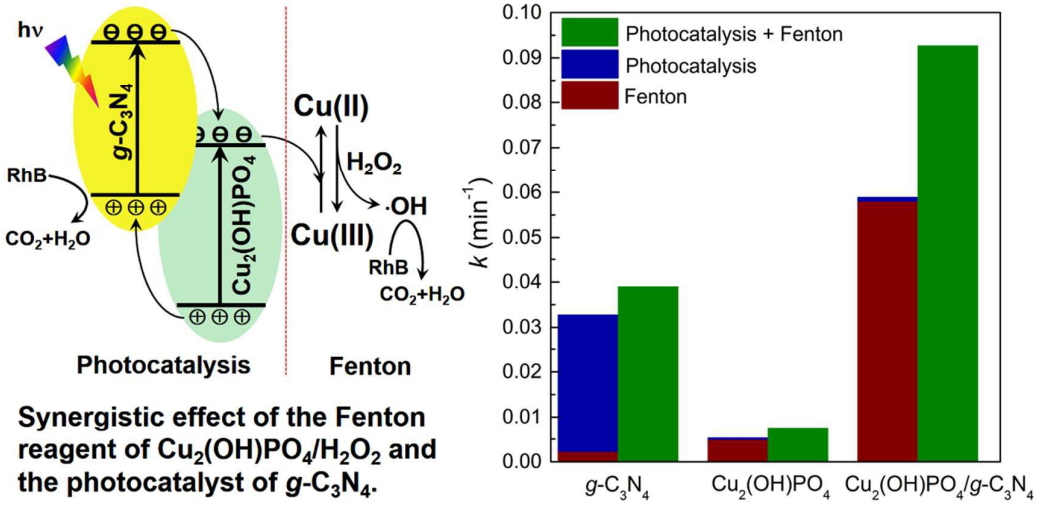

The synergistic effect of $Cu_2(OH)PO_4/H_2O_2$ and $g\text{-}C_3N_4$ highly boosts the catalytic activity towards photo-Fenton photocatalytic degradation of Rhodamine B.